Available online at www.sciencedirect.com
SCIENCE DIRECT
Surface Science 600 (2006) 2528–2542
SURFACE SCIENCE
www.elsevier.com/locate/susc

Formation of interface and surface oxides on supported Pd nanoparticles

T. Schalow, B. Brandt, M. Laurin, S. Schauermann, S. Guimond, H. Kuhlenbeck, J. Libuda *, H.-J. Freund

Fritz-Haber-Institut der Max-Planck-Gesellschaft, Faradayweg 4-6, 14195 Berlin, Germany

Received 18 January 2006; accepted for publication 13 April 2006
Available online 11 May 2006

Abstract

We have quantitatively studied the interaction between oxygen and an Fe_3O_4-supported Pd model catalyst by molecular beam (MB) methods, time resolved IR reflection absorption spectroscopy (TR-IRAS) and photoelectron spectroscopy (PES) using synchrotron radiation. The well-shaped Pd particles were prepared in situ by metal evaporation and growth under ultrahigh vacuum (UHV) conditions on a well-ordered Fe_3O_4 film on Pt(1 1 1).

It is found that for oxidation temperatures up to 450 K oxygen predominantly chemisorbs on metallic Pd whereas at 500 K and above ($\sim 10^{-6}$ mbar effective oxygen pressure) large amounts of Pd oxide are formed. These Pd oxide species preferentially form a thin layer at the particle/support interface, stabilized by the iron-oxide support. Their formation and reduction is fully reversible. Upon decomposition, oxygen is released which migrates back onto the metallic part of the Pd surface. In consequence, the Pd interface oxide layer acts as an oxygen reservoir, the capacity of which by far exceeds the amount of chemisorbed oxygen on the metallic surface.

Additionally, Pd surface oxides can also be formed at temperatures above 500 K. The extent of surface oxide formation critically depends on the oxidation temperature. This effect is addressed to different onset temperatures for oxidation of the particle facets and sites. It is shown that the presence of Pd surface oxides sensitively modifies the adsorption and reaction properties of the model catalyst, i.e. by lowering the CO adsorption energy and CO oxidation probability. Still, a complete reduction of the Pd surface oxides can be obtained by extended CO exposure, fully reestablishing the metallic Pd surface.

Keywords: Palladium; Iron-oxide; Oxidation; Surface oxide; CO; Model catalyst; Molecular beam; IR reflection absorption spectroscopy; Photoelectron spectroscopy

1. Introduction

In heterogeneous catalysis, oxide-supported metal nanoparticles are commonly used as catalysts for a variety of reactions [1,2]. Often, it is found that activity and selectivity of such supported catalysts are critically controlled by the surface structure and morphology of the active metal particles as well as by interactions between metal particles and oxide support. Consequently, structural changes of the catalyst at the microscopic level may sensitively modify its activity. In particular on transition metal surfaces in environments containing oxygen, major structural changes may occur, connected to the formation of different oxide species, e.g. chemisorbed oxygen, surface oxides or bulk metal oxides [3–17]. It has been shown that the formation of such surface oxides is associated with significant changes in the activity of single crystal surfaces [18–20]. In most cases, the mechanism of oxidation and the role of the various species in catalytic reactions are only poorly understood. The situation becomes further intricate for supported metal particles considering, e.g. the simultaneous presence of different sites, such as defects, edges, corners, different facets, modified lattice and electronic

* Corresponding author. Present address: Lehrstuhl für Physikalische Chemie II, Universität Erlangen-Nürnberg, Egerlandstr. 3, D-91058 Erlangen, Germany. Tel.: +49 9131 85 27308; fax: +49 9131 85 28867.
E-mail address: joerg.libuda@chemie.uni-erlangen.de (J. Libuda).

0039-6028/$ - see front matter © 2006 Elsevier B.V. All rights reserved.
doi:10.1016/j.susc.2006.04.016

properties and metal/support interactions. It is important to point out that many features of dispersed nanoparticle systems cannot be modeled on the basis of single crystal surfaces. Therefore, corresponding studies require the use of complex nanoparticle-based model surfaces [21,22].

In this contribution we present a comprehensive study on the interactions between oxygen and iron-oxide supported Pd nanoparticles. It is found that different oxygen species, i.e. chemisorbed oxygen, surface oxides and interface oxides, can be formed depending on the oxidation temperature. Their formation kinetics and their catalytic activity towards CO oxidation is studied at a detailed level combining several experimental factors:

First we use well-ordered oxide-film-supported model catalysts, which provide clean and well-defined surfaces and a strongly reduced level of complexity as compared to real catalysts (see e.g. [22–26] for recent reviews on model catalysts). These systems are compatible with various standard surface science techniques and can be characterized at the atomic level. Secondly, we have employed multi-molecular beam methods (MB), time resolved IR reflection absorption spectroscopy (TR-IRAS) and high-resolution photoelectron spectroscopy (PES) using synchrotron radiation in order to probe the formation of the different oxygen species (see e.g. [22]). This approach enables us to quantitatively study the oxygen uptake and release of the model catalyst and to characterize the oxygen species formed under well-defined conditions. Simultaneously, the Pd surface is characterized by TR-IRAS experiments using CO as a surface sensitive probe molecule.

Recently, we have shown for a Pd/Fe_3O_4 model catalyst that initial oxidation of the Pd particles occurs by formation of a thin Pd oxide layer at the particle/support interface [27]. This oxide layer, which can be reversibly accumulated and depleted, acts as an oxygen reservoir providing oxygen for surface reactions. In this contribution we quantitatively study the formation of different oxygen species in detail and over a broad range of temperatures. While mostly oxygen chemisorption on metallic Pd was found upon oxygen exposure below 450 K, large amounts of Pd oxide at the particle/support interface are formed at 500 K. For oxidation temperatures beyond 500 K, Pd surface oxides have also been observed, which drastically modify the adsorption properties of the catalyst. However, their formation sensitively depends on the oxidation temperature as a result of kinetic hindrances. Both Pd surface oxides and interface oxides can be reduced by extended CO exposure resulting in the formation of CO_2.

2. Experimental

All MB and IRAS experiments were performed in a UHV apparatus at the Fritz-Haber-Institut (Berlin), which has recently been described in the literature [28]. The system offers the experimental possibility of crossing up to three beams on the sample surface. A schematic representation of the setup is shown in Fig. 1. The effusive beams were generated by doubly differentially pumped sources based on multi-channel arrays and modulated using remote-controlled shutters. Typical beam intensities were between 2.1×10^{14} and 1.1×10^{15} molecules $cm^{-2}\,s^{-1}$. Both sources were operated at room temperature. The beam diameter of the effusive sources was chosen such that it exceeds the sample surface. The supersonic beam was generated by a triply differentially pumped source from a supersonic expansion and modulated by a solenoid valve and a remote-controlled shutter. The beam intensity was 4.6×10^{14} molecules $cm^{-2}\,s^{-1}$ in all cases. The beam diameter was chosen smaller than the sample for MB titration experiments whereas a beam diameter matching the size of sample and exceeding it was chosen for pulsed oxygen adsorption and IRAS experiments, respectively. All experiments have been performed using $^{18}O_2$ (Campro Scientific, 95% ^{18}O, 99.7% purity), $^{16}O_2$ (Linde, 99.999%) and $C^{16}O$ (Linde, 99.997% further purified by a gas filter (Mykrolis)). For gas-phase detection an automated QMS system (ABB Extrel) was employed. IR spectra were acquired by a

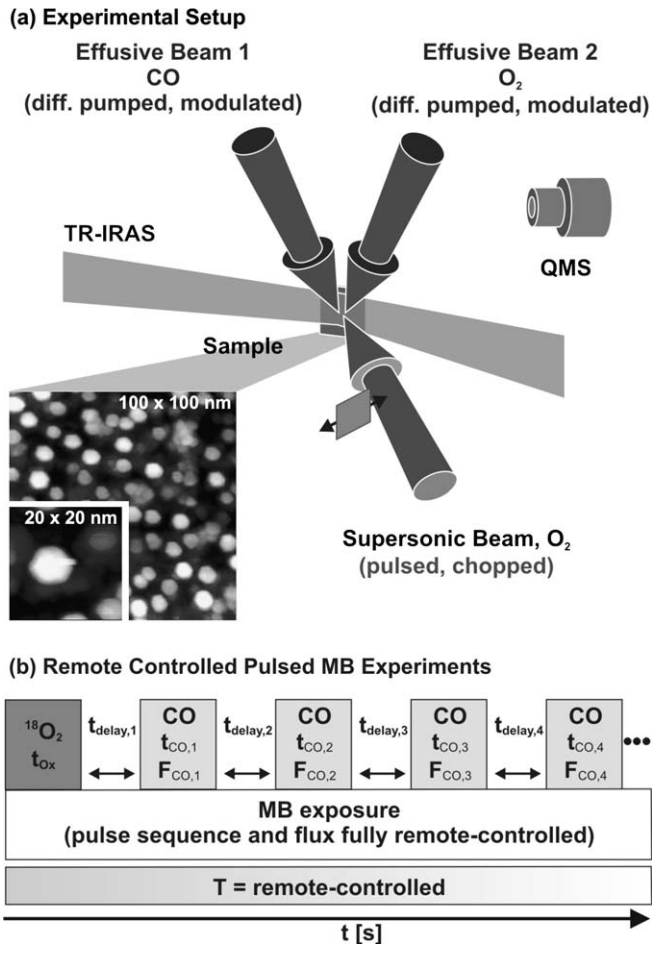

Fig. 1. (a) Schematic representation of the molecular beam setup and STM image of the model catalyst used in this study (STM of Pd/Fe_3O_4 by Starr and Shaikhutdinov [31]). (b) Illustration of the pulse and temperature sequence of the remote-controlled molecular beam experiments.

vacuum FT-IR spectrometer (Bruker IFS 66v/S) with a spectral resolution of 2 cm^{-1}, using an MIR polarizer to select the p-component of the IR light only.

PES experiments have been performed in a separate chamber at BESSY II, beamline UE52-PGM1. The chamber was equipped with standard sample cleaning/preparation facilities. PES spectra were taken using a 200 mm hemispherical energy analyzer (Scienta SES200). The energy resolution was ~100 meV at $h\nu = 465$ eV and ~160 meV at $h\nu = 840$ eV.

The thin (~100 Å) Fe_3O_4 film was grown on Pt(1 1 1) by repeated cycles of Fe (>99.99%, Goodfellow) deposition and subsequent oxidation (see [29,30] for details). Cleanliness and quality of the oxide film were checked by IRAS of adsorbed CO (for MB experiments), PES (for PES experiments) and LEED. Pd particles (>99.9%, Goodfellow) were grown by physical vapor deposition (Pd coverage: 2.7×10^{15} atoms cm^{-2}, sample temperature: 115 K) using a commercial evaporator (Focus, EFM 3, flux calibrated by a quartz microbalance). Directly after Pd deposition, the sample was annealed at 600 K and stabilized by 5 cycles of oxygen exposure (8×10^{-7} mbar for 1000 s) and subsequent CO exposure (8×10^{-7} mbar for 3000 s) at 500 K to form well-shaped crystalline Pd particles unless otherwise stated. An STM image of the model surface is shown in Fig. 1.

3. Results and discussion

3.1. Experimental setup and model system

The experimental approach applied in this study to probe the interactions between oxygen and Pd nanoparticles under well-controlled reaction conditions is summarized in Fig. 1a: Employing molecular beam methods, TR-IRAS and PES the formation and catalytic activity of different oxygen species on supported Pd model catalysts is comprehensively investigated.

Specifically, we have studied Pd particles prepared in situ under ultrahigh vacuum conditions (UHV) on a thin (~100 Å), well-ordered Fe_3O_4 film as a support. Prior to the experiments, the sample has been repeatedly oxidized and reduced to obtain a stable surface under the conditions of all experiments presented in this study [31]. Structure and adsorption properties of the oxide support and Pd particles have been investigated in detail previously [30,31]. Briefly, the well-shaped Pd crystallites, which have an average diameter of about 7 nm and contain approximately 3000 atoms, cover the support uniformly with an island density of about 8.3×10^{11} islands cm^{-2} (Pd coverage: 2.7×10^{15} atoms cm^{-2}). They grow in (1 1 1) orientation with respect to the support and predominately expose (1 1 1) facets (~80%) but also a smaller fraction of (1 0 0) facets (~20%). An STM image of the model catalyst is shown in Fig. 1a.

In order to quantitatively probe the interactions between oxygen and the model catalyst, a variety of fully automated, remote-controlled pulsed MB experiments has been performed. This versatile technique enables us to exactly quantify even small amounts of oxide species formed on the catalysts surface in a very reproducible fashion. A typical pulse and temperature sequence of such an experiment is shown in Fig. 1b: First the sample is exposed to an oxygen pulse at a defined temperature to form certain oxygen species on the catalyst surface. After an adjustable delay time, in which the sample temperature can be changed, CO pulses are applied to probe the formation of different oxygen species by means of CO oxidation to CO_2. CO_2 desorbs instantaneously and can be detected in the gas-phase by a QMS. Such pulsed MB CO titration experiments allow an accurate quantification of the CO_2 yield even for very low reaction probabilities. The CO flux, pulse duration and delay time between the pulses can be individually controlled for each pulse to gain detailed insights into the reaction kinetics of the different oxygen species. Simultaneously, TR-IRAS spectra of adsorbed CO are acquired to characterize the catalyst surface in situ during the reduction. Due to the variety of parameters, which can be individually controlled, their versatility and reproducibility, these automated MB experiments allow us to study different aspects of the oxide formation and reduction on supported Pd nanoparticles and to elucidate the reaction mechanisms involved.

3.2. Oxide formation and quantification

As a first step to study the interactions between the surface of the model catalyst and oxygen, pulsed MB titration experiments have been performed at different surface temperatures. The pulse and temperature sequence of such an experiment is shown in Fig. 2a: First the sample is exposed to a pulse of oxygen (1.7×10^{-6} mbar for 100 s: 130 L (1 L oxygen corresponds to 3.6×10^{14} molecules cm^{-2})). After a short delay time (10 s), pulses of CO (5 s on-time, 5 s off-time, 8×10^{-7} mbar: 3 L per pulse) were applied to probe the oxygen release by CO oxidation to CO_2, which desorbs immediately and can be detected in the gas-phase. All MB titration experiments have been performed using a supersonic $^{18}O_2$ beam. In Fig. 2b, the CO_2 formation rate of a pulsed MB titration experiment at 500 K is shown. Here, the CO_2 formation rate shows a bimodal behavior: The reaction rate is high for the very first CO pulse while it is noticeably slower but still finite for up to 100 following pulses. By integrating the CO_2 formation over all CO pulses applied, the total amount of oxygen withdrawn out of the sample can easily be estimated from this experiment. The integral oxygen release for pulsed MB titration experiments at different surface temperatures is shown in Fig. 2c. Interestingly, the total oxygen storage capacity of the model catalyst at 500 K is nearly four times and at 600 K nearly five times higher compared to the amount of oxygen stored at 400 K. From the steeper slope of the oxygen release (see Fig. 2c) during the first few CO pulses at 500 K compared to 600 K, it can be derived that the rate

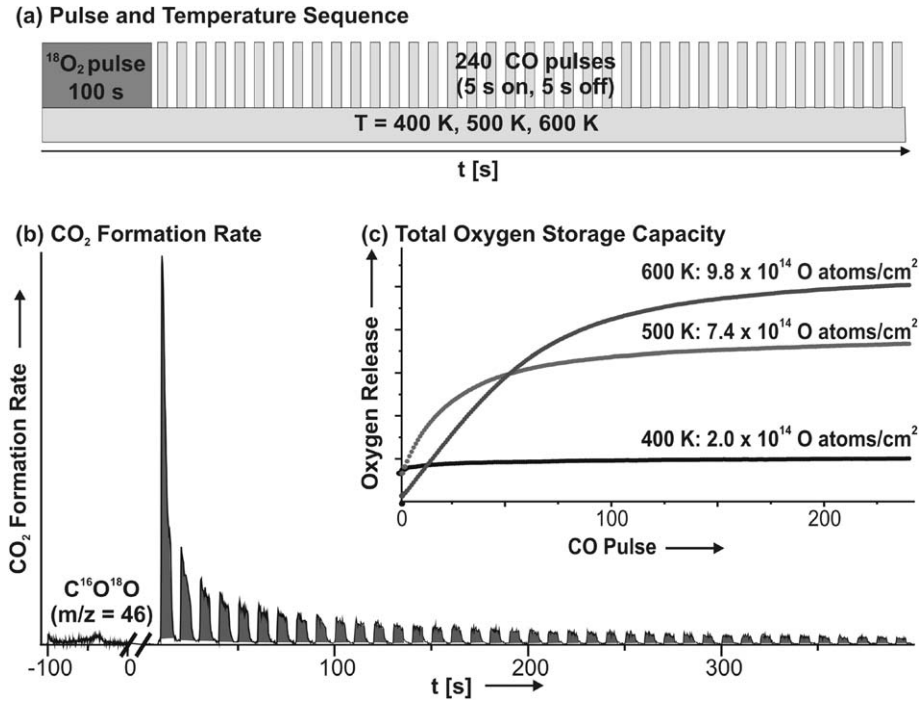

Fig. 2. (a) Pulse and temperature sequence of the CO titration experiments: First the sample is exposed to an oxygen pulse (1.7×10^{-6} mbar, 100 s, 130 L). Subsequently 240 CO pulses (5 s on-time (8×10^{-7} mbar, 3 L), 5 s off-time) are applied to withdraw oxygen stored in the catalyst in form of CO_2; (b) CO_2 formation rate for a surface temperature of 500 K and (c) integral oxygen release for different surface temperatures.

of CO oxidation is drastically slower at 600 K even though the total amount of oxygen stored is significantly higher.

In Pd single crystal studies it has previously been shown that oxygen mainly adsorbs dissociatively up to 400 K forming an ordered overlayer of chemisorbed oxygen [3,32]. For oxidation temperatures beyond 500 K, however, the formation of surface oxides has been recently reported for various Pd single crystal surface (see e.g. [13,14] and references therein). These surface oxides involve major reconstructions of the Pd surface and their oxygen density ($\theta \sim 1$, see e.g. [12,13]) by far exceeds the density of chemisorbed oxygen overlayers.

Accordingly, we explain the large oxygen uptake above 500 K by the formation of Pd oxide species while the amount of oxygen stored at 400 K is assigned to chemisorbed oxygen only. In order to estimate the oxygen storage capacity of the model catalyst from the pulsed CO titration experiment, we proceed as follows: The amount of Pd surface atoms can be determined by CO sticking coefficient measurements at 300 K. Under these conditions CO adsorbs on Pd particles with a coverage $\theta \sim 0.50$ (Pd(1 1 1), Pd(1 0 0): $\theta = 0.50$ [33]) and the CO adsorption was found to be 3.0×10^{14} molecules cm^{-2}. Consequently, we assume the number of Pd surface atoms to be $6.0 \times 10^{14}\ cm^{-2}$, which is twice the CO density at 300 K. This value is consistent with the number of Pd surface atoms estimated on the basis of STM data. For oxygen chemisorption on Pd particles an average coverage of $\theta \sim 0.30$ (80% Pd(1 1 1): $\theta = 0.25$ [3]; 20% Pd(1 0 0): $\theta = 0.50$ [32]) is expected. Therefore we assume the amount of chemisorbed oxygen that can be adsorbed on the Pd particles to be 2×10^{14} atoms cm^{-2}. As discussed above, oxygen exposure at 400 K results mainly in the formation of a chemisorbed oxygen overlayer. Hence the oxygen release at 400 K should amount to 2×10^{14} atoms cm^{-2}. At 600 K, an oxygen storage capacity of 9.8×10^{14} atoms cm^{-2} is found. This value even exceeds the oxygen density which would be expected on the basis of the formation of a surface oxide [13,14]. Therefore, it is reasonable to assume that, in addition to the formation of surface oxides, additional parts of the nanoparticles must be oxidized. Considering the high density of irregular sites, e.g. corner, steps or defects, and, as we will show later, the presence of a metal–support interface, it is reasonable to assume a higher susceptibility to oxidation of Pd particles, as compared to a regular single crystal surface.

It is noteworthy to point out that the kinetics of oxygen release during the first few CO pulses at 600 K is significantly slower than at 400 K, even though larger total amounts of oxygen are accumulated at 600 K. In view of the bimodal behavior of the CO_2 formation rate at 500 K, it can be concluded that there are two different oxygen species present, which facilitate the CO oxidation:

The first oxygen species shows a high reaction probability and, therefore, a fast CO oxidation kinetics. It is rapidly depleted, governing the CO_2 formation rate at 400 K and during the first CO pulse at 500 K. Since at 400 K, nearly all oxygen is present in form of chemisorbed oxygen, we attribute this contribution to chemisorbed atomic oxygen on metallic Pd surface areas. This assignment is in good

agreement with previous studies where a high reaction probability and fast depletion of chemisorbed oxygen for CO oxidation was found [34,35]. Hence, the CO_2 yield of the first CO pulse can be interpreted as the amount of chemisorbed oxygen available on the metallic Pd surface. At 600 K the amount of chemisorbed oxygen is ~85% lower than at 400 K suggesting an almost complete coverage of the Pd surface by surface oxides (see Fig. 2c) whereas at 500 K the amount of chemisorbed oxygen is only slightly reduced as compared to 400 K. Therefore we assume the surface to be primarily metallic at 500 K.

The second oxygen species exhibiting a lower reaction probability for CO oxidation, which controls the kinetics at 600 K, must, therefore, be attributed to the Pd oxide species. Comparing the kinetics of CO oxidation involving Pd oxide for a mainly metallic Pd surface (500 K) and for a largely oxidized Pd surface (600 K), it is found that the oxygen release is slower if more Pd surface oxide is formed. This finding indicates that the reaction probability for CO with the Pd oxide species is low. Instead, we suggest that CO oxidation mainly proceeds via slow decomposition of the oxide, releasing oxygen onto metallic Pd areas, where it rapidly reacts with CO. This mechanism is in agreement with transient molecular beam experiments, in which the activity of Pd oxide species and chemisorbed oxygen was probed individually [36]. A second surprising observation is related to the amount of oxygen released from the Pd oxide at 500 K. In spite of the fact that most of the surface remains metallic under these conditions, the total oxygen yield from the oxide exceeds the amount of chemisorbed oxygen by a factor of three, at least. This observation indicates that oxidation does not primarily occur at the outer surface of the Pd particles. In fact, we will show below that initial oxidation preferentially occurs at the Pd/support interface, allowing large amounts of oxygen to be stored without substantially affecting the metallic character of the outer particle surface.

In the next step we have studied the kinetics of oxide formation on the model catalyst. Here, the oxygen exposure during the pulsed MB CO titration experiments is varied at constant surface temperature of 500 K. The pulse and temperature sequence of theses experiments is shown in Fig. 3a: Again, the sample is first exposed to an oxygen pulse of variable duration (1.7×10^{-6} mbar, 1.3 L/s; 1–1000 s) and subsequently titrated by 360 CO pulses (5 s on-time, 5 s off-time, 8×10^{-7} mbar: 3 L per pulse). The average CO_2 yield of the last 60 pulses, which is assumed to be dominated by background contributions, is subtracted for each pulse as a background correction. In Fig. 3b the oxygen release is shown for different oxidation times at 500 K. The total oxygen release (corresponding to the amount of oxide reversibly formed on the particles) as a function of oxidation time is depicted in Fig. 3c. While in the beginning a steep increase is observed, the oxide forma-

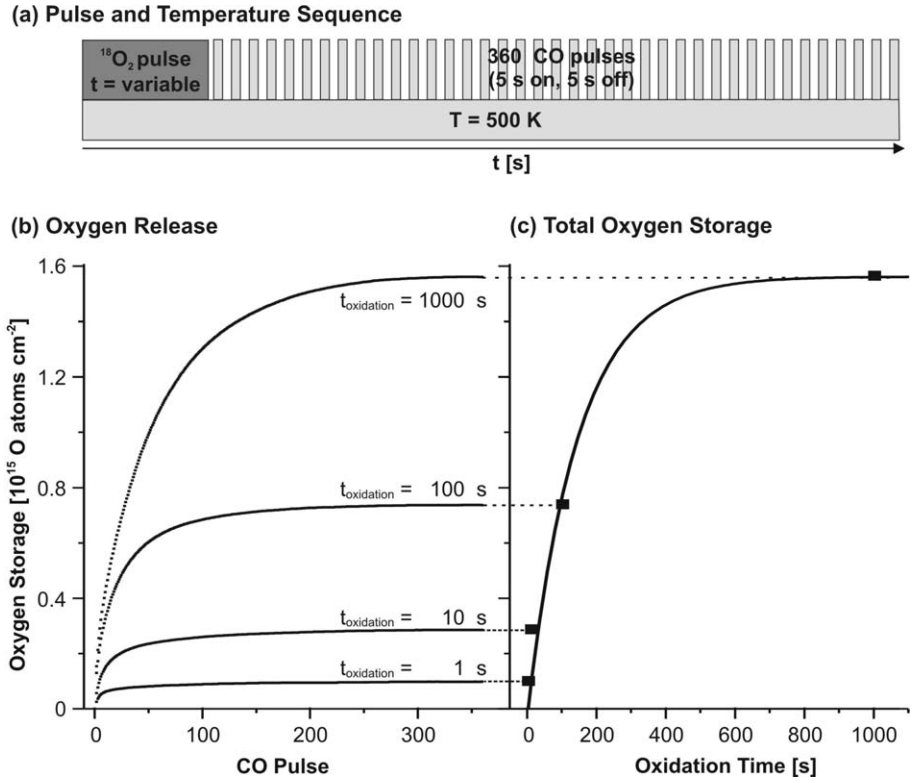

Fig. 3. (a) Pulse and temperature sequence of the CO titration experiments: First the sample is exposed to an oxygen pulse (1.7×10^{-6} mbar, 1–1000 s, 1.3 L/s). Subsequently 360 CO pulses (5 s on-time (8×10^{-7} mbar, 3 L), 5 s off-time) are applied to withdraw oxygen; (b) integral oxygen release for different oxygen exposures and (c) total oxygen storage capacity as a function of oxygen exposure.

tion becomes significantly slower after an oxygen exposure of about 250 s and finally reaches its saturation at a nominal oxygen density of about 1.5×10^{15} O atoms cm^{-2}. Note that for other particle sizes a similar saturation behavior has been observed.

The finite oxygen storage capacity shown in Fig. 3c fits well to the limited amount of Pd available for oxidation on the catalyst surface. However, the saturation oxygen storage capacity at 500 K corresponds to a O/Pd stoichiometry of approximately 0.55. Apparently, a complete oxidation of the Pd particles under the conditions applied is not possible. This is in accordance with the finding that after oxidation at 500 K most of the Pd surface still remains metallic. We suggest that specific parts of the Pd particles, i.e. specifically the particle/support interface as shown later, are more susceptible to oxidation whereas oxidation of the well-ordered facets is kinetically inhibited. The decreasing rate of oxide formation with increasing oxygen exposure (see Fig. 3c) can be attributed to kinetic limitations successively hindering the oxidation.

The CO titration experiments can only provide information on the oxygen release. In order to directly quantify the oxygen uptake, we would have to perform oxygen sticking coefficient measurements at different surface temperatures. Here we are facing an experimental difficulty: The initial oxygen sticking probability on the metallic Pd is high, but decreases to a very low value as the chemisorbed oxygen layer approaches saturation. Oxide formation itself is slow and occurs from the nearly saturated chemisorbed layer, which itself is replenished by chemisorption. The result is a very low sticking probability, which cannot be precisely determined via a conventional King and Wells experiment [37,38]. Instead we perform a pulsed oxygen adsorption experiment in order to quantify the oxygen uptake. Here, it is taken advantage of the fact that in a pulsed experiment exposure and reaction time are decoupled at constant flux. The pulse and temperature sequence of such an experiment is shown in Fig. 4a: Short but intense pulses of oxygen ($^{16}O_2$, 1100 pulses, 1 s on-time, 4 s off-time, 1.7×10^{-6} mbar, 1.3 L) modulated by a computerized beam shutter are applied at open and closed shutter in an alternating sequence. The signal at closed shutter provides a reference for the chamber response to the gas pulse. If oxygen adsorbs on the surface the uptake can be determined from the QMS difference signal between sample and reference (see Fig. 4b, note that the scattering geometry and, therefore, the oxygen signal is slightly different for oxygen pulses applied onto the sample and onto the shutter). On Pd particles a dynamic equilibrium between chemisorbed oxygen and Pd oxide is established, strongly favoring the latter [36]. Thus, a fraction of the chemisorbed oxygen is converted to Pd oxide during the wait time in between the pulses. The converted oxygen is rapidly replenished during the next pulse, leading to a higher sticking probability as compared to a continuous beam experiment. Still, the total oxygen uptake accounts for less than 1% of the total oxygen dose, requiring to accumulate several runs in an automated experiment in order to obtain a reasonable signal-to-noise ratio. In order to calculate the oxygen adsorption per pulse as precisely as possible, each pulse impinging on the sample is first normalized with respect to the adjacent oxygen pulses impinging on the shutter. This procedure allows us to correct for small variations in beam intensity. In a second step, the oxygen uptake of the Pd/Fe_3O_4 model surface is determined by subtracting the reference from a clean Fe_3O_4 sample without Pd (see Fig. 4b). The integral oxygen uptake for different surface temperatures is shown in Fig. 4c. It is found that the oxygen uptake at 500 K exceeds the oxygen adsorption for the lower surface temperatures by a factor of about six.

At 300 K, the oxygen adsorption capacity, experimentally determined by the pulsed sticking coefficient measurement fits well to the amount of chemisorbed oxygen estimated on the basis of a conventional King and Wells type experiment [37,38] with CO (2×10^{14} atoms cm^{-2}). The slightly larger oxygen uptake at 400 K may be addressed to the formation of oxide species formed at sites more susceptible to oxidation, e.g. defects and (1 0 0) facets. Still, the oxygen uptake at 400 K is mainly due to dissociative chemisorption of oxygen. In analogy to the pulsed CO titration experiments, a large increase in oxygen storage capacity is observed upon increasing the surface temperature to 500 K. The absolute value derived from the adsorption experiments (1.7×10^{15} atoms cm^{-2}) agrees well with the oxygen release during the CO titration experiments for saturated Pd particles (1000 s O_2 exposure). These results show that oxidation of the Pd particles by O_2 and reduction by CO are fully reversible. PES spectra of the Pd 3d region also demonstrate that the Pd particles can be fully reduced after oxidation at 500 K by extended CO exposure. The O/Pd stoichiometry of ~0.6 estimated from the adsorption and titration experiments, on the other hand, indicates that there is no complete oxidation of the Pd particles under the conditions applied.

3.3. Oxide characterization

In the previous paragraph we have shown that at temperatures above 500 K significant amounts of Pd oxide can be formed on supported Pd nanoparticles. However, a complete oxidation of the entire Pd particle is not possible even after extended oxygen exposure at 500 K. We have therefore suggested that under these conditions only specific parts of the Pd particles become oxidized whereas others still remain metallic. The question arises which parts of the particles are initially oxidized and thus mainly facilitate the oxygen storage mechanism.

In order to characterize the oxidation state of the Pd surface and study the formation of Pd surface oxides, IRAS experiments using CO as a surface sensitive probe molecule have been performed. In Fig. 5a the pulse and temperature sequences of theses experiments are displayed: First the reduced sample was exposed to an oxygen pulse of

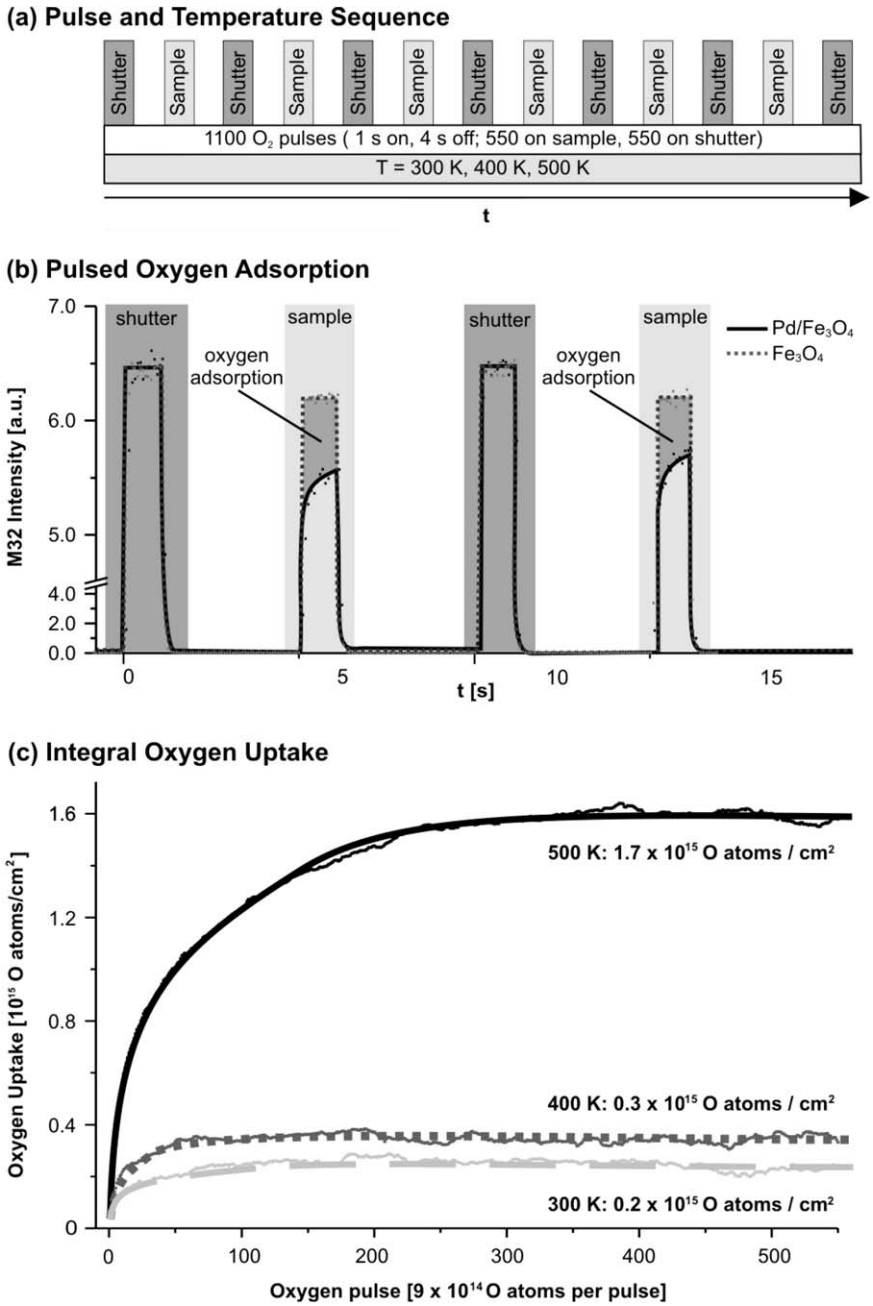

Fig. 4. (a) Pulse and temperature sequence of the pulsed oxygen adsorption experiments: 1100 oxygen pulses (1 s on-time (1.7×10^{-6} mbar, 1.3 L), 4 s off-time) are applied alternating on the sample and on a shutter covering the sample at different temperatures; (b) first oxygen pulses applied on a Pd/Fe_3O_4 and an Fe_3O_4 sample at 500 K and (c) integral oxygen uptake for different surface temperatures.

variable duration (8×10^{-7} mbar, 0.6 L/s, 1–10 000 s) at 500 K to form Pd oxide. Subsequently, the sample is cooled to 250 K in O_2 in order to form a saturated chemisorbed oxygen layer on the remaining metallic Pd surface. After further cooling to 125 K in UHV, the sample was saturated with CO and IRAS spectra of the CO/O co-adsorption layer were acquired. For CO/O co-adsorption on Pd(1 1 1) a well-ordered $p(2 \times 2)_{O+CO}$ structure was recently reported [39]. In Fig. 5b IRAS spectra of the CO stretching frequency region are displayed for different oxidation times at 500 K, consisting of a sharp peak at 2133 cm^{-1} and a broad feature at about 1960 cm^{-1} (see e.g. [40] for CO/O co-adsorption on Pd particles). With increasing oxygen exposure the intensity of these two features decreases while no additional features in the spectra and no shifts of the existing peaks can be observed. The integral IR intensities of both CO features after different oxygen exposures at 500 K are shown in Fig. 5c (normalized to the spectrum taken after oxygen exposure at 300 K, i.e. under conditions where no formation of surface oxides occurs). A pronounced decrease in intensity is observed for short oxygen exposures. With longer oxidation times the decrease

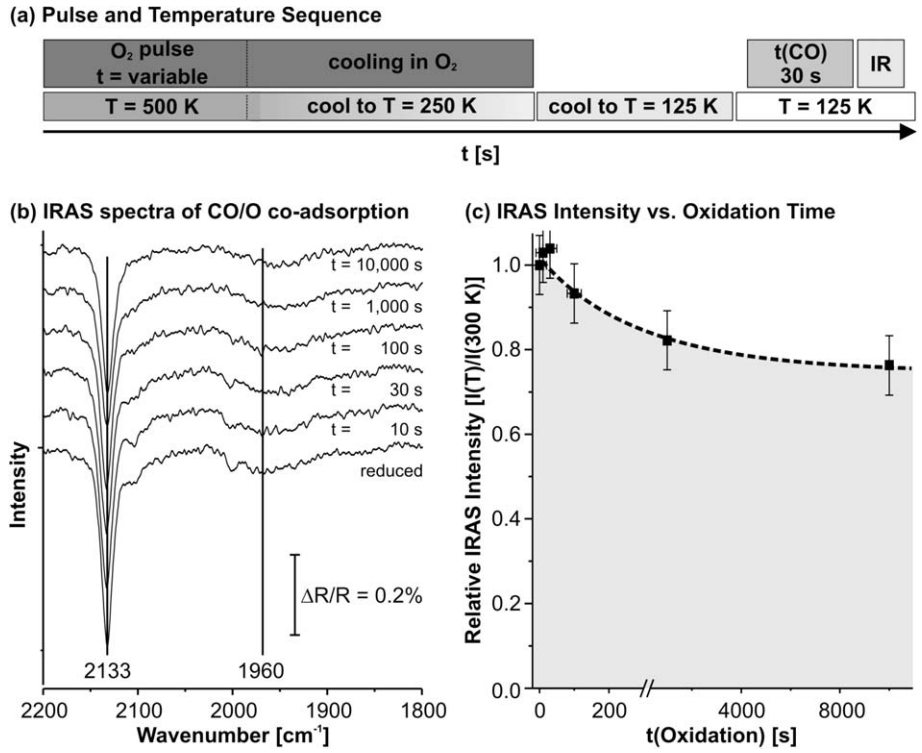

Fig. 5. (a) Pulse and temperature sequence of the IRAS experiments: First the sample is exposed to an O_2 pulse (8×10^{-7} mbar, 1–10 000 s, 0.6 L/s) and subsequently cooled in O_2 to 250 K. After further cooling in UHV to 125 K, the sample is exposed to CO (8×10^{-7} mbar, 30 s, 18 L) and IR spectra are taken; (b) IRAS spectra of the CO stretching frequency region for CO/O co-adsorption on Pd/Fe_3O_4 at 125 K for different oxygen exposures at 500 K and (c) integral IRAS intensity normalized on the reduced surface as a function of oxygen exposure.

becomes slower and finally settles at about 75% of the IRAS intensity obtained for the reduced surface.

From these experiments two main conclusions can be drawn: First, we assign the decreasing IRAS intensity to the formation of Pd surface oxides making the surface partially inert with respect to CO adsorption. This is in agreement with single crystal data reporting the formation of Pd surface oxides under similar conditions. Interestingly, no additional features, which could be associated with CO adsorption on Pd surface oxides, were observed upon oxidation. Therefore we conclude that CO does not adsorb on surface oxides under the conditions ($T = 125$ K, $p_{CO} \sim 10^{-6}$ mbar) applied in these experiments. Secondly, the CO adsorption cannot be completely quenched by oxidation of the Pd particles at 500 K. Instead, a remaining IRAS intensity for CO adsorption of ~75% was found even after extended oxygen exposure at $\sim 10^{-6}$ mbar. This observation indicates that the particles are still mainly terminated by a metallic surface. In contrast, oxidation at 600 K results in a nearly complete disappearance of all IR features for CO adsorption as will be shown later. Obviously, only a minor fraction, e.g. specific sites more susceptible to oxidation, but not the entire Pd particles surface is oxidized at 500 K ($\sim 10^{-6}$ mbar). This effect can be attributed to kinetic hindrances inhibiting the formation of surface oxides on part of the Pd particles (compare [15]). As a result, partially oxidized Pd nanoparticles, on which metallic surface areas and surface oxides co-exist, are formed upon oxygen exposure at 500 K. Note that despite the low degree of surface oxidation, large amounts of oxygen can be stored in the Pd particles at 500 K. Consequently, the oxygen storage functionality of the model catalyst cannot be linked to the formation of Pd surface oxides alone.

To characterize the different oxygen species in more detail we have performed high-resolution PES experiments using synchrotron radiation. The surface sensitivity of the PES spectra can be controlled by varying the photon energy. For increasing photon energies $h\nu$ the kinetic energy of the emitted photoelectrons increases and so does the electron escape depth λ ($h\nu = 465$ eV, $\lambda \approx 4$ Å; $h\nu = 840$ eV, $\lambda \approx 9$ Å [41]). As a result, bulk features become more pronounced for higher photon energies while surface features contribute more relative intensity for lower photon energies.

In Fig. 6, PES spectra of the Pd $3d_{5/2}$ region of the model catalyst after different preparation steps are shown. In these experiments the sample has not been stabilized by repeated oxidation/reduction cycles but it has been annealed at 600 K prior to the experiments. The upper spectra (Fig. 6a) have been taken directly after preparation of the model catalyst. Here, the Pd $3d_{5/2}$ region can be decomposed into one component at a binding energy (BE) of 335.0 eV and another component at a BE of 335.2 eV. The lower BE feature is more pronounced at lower PE (photon energy, $h\nu = 465$ eV) and the higher BE feature at higher PE ($h\nu = 840$ eV).

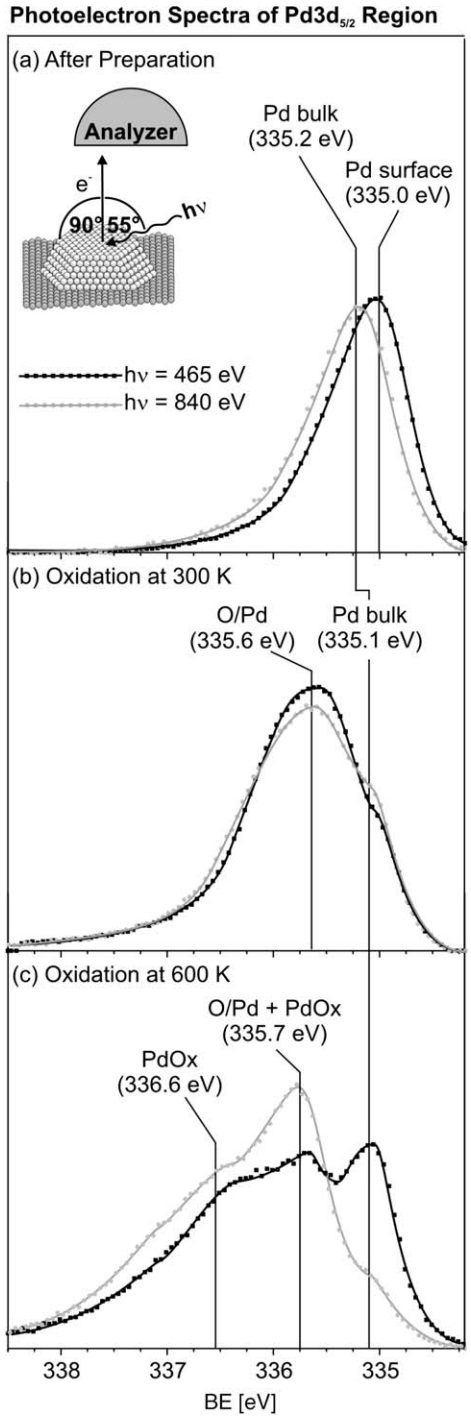

Fig. 6. High-resolution photoelectron spectra of Pd $3d_{5/2}$ region at different photon energies: (a) immediately after Pd deposition and annealing in UHV to 600 K; (b) after oxygen exposure at 300 K (oxygen dose: 8×10^{15} molecules cm^{-2}) and (c) after oxygen exposure at 600 (oxygen dose: 3×10^{17} molecules cm^{-2}).

According to the literature, we assign the higher BE feature (~335.2 eV) to metallic bulk Pd and the lower BE feature (~335.0 eV) to Pd surface atoms [42]. A more accurate assignment of the features to individual Pd species is not reasonable because of the high complexity of the model catalyst and the abundance of different sites compared to single crystals. However, the surface core-level shift (SCLS) of ~0.2 eV compared to the bulk is in good agreement with single crystal studies on Pd(1 1 1) [42]. As expected the surface-derived component is more prominent for lower PE whereas the bulk component becomes more dominant at higher PE.

In Fig. 6b PES spectra taken after oxygen exposure at 300 K (1×10^{-7} mbar, 200 s, 15 L) are shown. The resulting spectra consists of a lower BE feature at 335.1 eV and an additional peak at a BE of 335.6 eV. Here, the lower BE feature contributes more intensity at a higher PE and the higher BE feature at a lower PE.

At 300 K oxygen chemisorbs dissociatively on Pd particles forming an order overlayer of atomic oxygen (Pd(1 1 1): p(2 × 2), $\theta = 0.25$ [3]; Pd(1 0 0): c(2 × 2), $\theta = 0.50$ [32]). Therefore, the higher BE component (~335.6 eV) can be assigned to Pd surface atoms coordinated to adsorbed oxygen and the lower BE component (335.1 eV) to metallic bulk Pd. A shift of 0.5 eV in BE for Pd atoms coordinated to adsorbed oxygen with respect to bulk Pd is in agreement with Pd single crystal studies for oxygen adsorption [14,43]. Comparing the PES spectra for the different PEs, it can clearly be seen that the lower BE component, which we have previously assigned to metallic Pd, is more pronounced for the higher PE. This agrees well with what is expected for the formation of a chemisorbed oxygen layer on the surface of the Pd particles.

In order to characterize the Pd oxide, PES spectra have also been taken after oxidation of the Pd particles at 600 K (1×10^{-6} mbar, 1000 s, 750 L, see Fig. 6c). Here the spectra consist of mainly three different features: A lower BE feature at 335.1 eV, an intermediate BE region at about 335.7 eV and a higher BE shoulder at about 336.6 eV. The lower BE component is much more pronounced in the more surface sensitive spectrum taken at low PE whereas the shoulder at higher BE is contributing more intensity in the bulk sensitive spectrum at high PE.

The pulsed CO titration experiments discussed in the previous paragraph have shown that after oxidation at 600 K large amounts of Pd oxide species are formed. Consequently we assign the intermediate BE component at ~335.7 eV to metallic Pd coordinated to adsorbed oxygen and to specific Pd atoms in a thin Pd oxide and the higher BE shoulder at ~336.6 eV to Pd oxide exclusively. This assignment is in agreement with BEs which have recently been reported for Pd oxide in single crystal studies [13,14]. As discussed above, the low BE feature at ~335.1 eV is assigned to metallic Pd. Note that a more detailed assignment of the different components is precluded due to the large number of nonequivalent sites.

Two important conclusions can be drawn from these spectra: First the BE of the metallic Pd peak is not shifted with respect to the reduced system upon oxidation indicating that the nature of the particle core still remains metallic. Therefore, it appears unlikely that massive oxygen dissolution in the Pd lattice is responsible for the oxygen storage mechanism. This result is in agreement with recent theoretical studies [16]. The most striking observation,

however, is the reduced intensity of the metallic Pd feature for the more bulk sensitive spectrum at higher PE. (In order to verify that these intensity changes are not due to photoelectron diffraction effects, PES measurements have also been performed at other photon energies. It should be noted that, in comparison to single crystal surfaces, diffraction effects are typically less pronounced on supported particle systems due to a lower degree of ordering.) Apparently, most of the Pd oxide is not formed at the outer particle surface (this would result in an increased intensity of the metallic signal for higher PE). Therefore, we suggest that the formation of Pd oxide species preferentially occurs at the particle/support interface and not on the particle surface, i.e. the particle/vacuum interface. As a driving force we suggest that there is a stabilization of the Pd oxide layer at the particle/support interface due to strong electrostatic interaction with the Fe_3O_4 support.

The stabilization of the interface oxide is further substantiated by transient molecular beam experiments showing that the formation of the Pd interface oxide layer is, in contrast to Pd surface oxides on single crystals, thermodynamically favorable in comparison to surface chemisorption [36]. Recently we have also shown that the formation of Pd oxide species is connected to a ripening of the particles, involving not only a reshaping of the particles but also a decrease in particle density and an increase in particle size [31]. This process we assume to be facilitated by mobile Pd oxide species also indicating strong interactions between Pd oxide species and the oxide support. Finally, the formation of a Pd interface oxide layer is also in agreement with the previously discussed CO titration and IRAS experiments, showing substantial oxide formation without a large effect on the metallic Pd surface. As discussed previously, the oxygen storage mechanism at the particle/support interface facilitates reversible storage and release of oxygen during surface reactions on the remaining metallic Pd surface [27].

Apart from Pd oxide formation, a second oxygen storage channel may be taken into account based on oxygen migration from the particles onto and into the support (oxygen spillover). This channel could give rise to further oxidation and reduction of the support. Such a process may appear particularly likely taking into account that Fe_3O_4 is a mixed valency oxide. In order to study the oxygen exchange between oxygen species on the Pd particles and the support, pulsed CO titration experiments were performed on an isotopically labeled $Fe_3{}^{18}O_4$ support (see Fig. 7a). For this purpose the sample was first

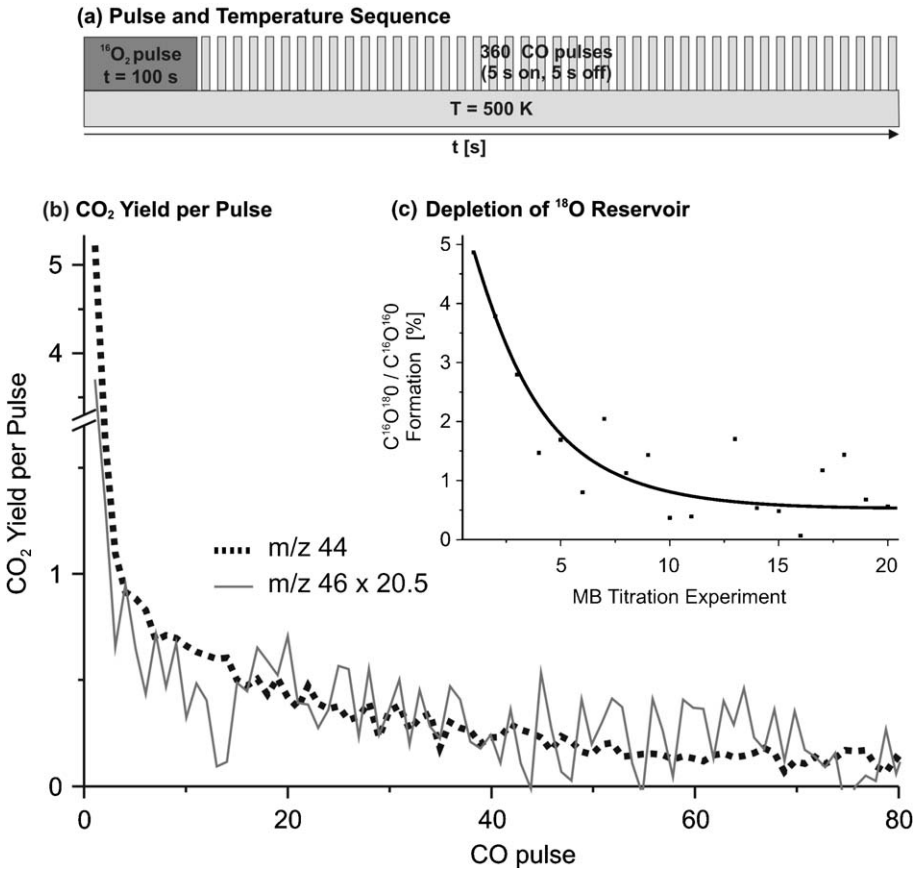

Fig. 7. (a) Pulse and temperature sequence of a CO titration experiment on an isotopically labeled $Fe_3{}^{18}O_4$ support: First the sample is exposed to an $^{16}O_2$ pulse (1.7×10^{-6} mbar, 100 s, 130 L). Subsequently 360 CO pulses (5 s on-time (8×10^{-7} mbar, 3 L), 5 s off-time) are applied to withdraw oxygen; (b) CO_2 yield per CO pulse for $C^{18}O^{16}O$ (scaled by 20.5) and $C^{16}O^{16}O$ and (c) overall isotopic ratio $C^{18}O^{16}O/C^{16}O^{16}O$ as a function of consecutively performed MB titration experiments.

exposed to a $^{16}O_2$ pulse (1.7×10^{-6} mbar, 130 L; 100 s) and subsequently titrated by 360 $C^{16}O$ pulses (5 s on-time, 5 s off-time, 8×10^{-7} mbar, 3 L per pulse). Note that these experiments were performed on a sample, which had not been stabilized by repeated oxidation/reduction cycles before, but which had been annealed to 600 K prior to the experiments. The CO_2 formation rate for $C^{16}O^{16}O$ and $C^{16}O^{18}O$ was detected individually by QMS. If large amounts of $^{16}O^{2-}$ ions could be stored in the $Fe_3{}^{18}O_4$ support lattice, scrambling with lattice $^{18}O^{2-}$ ions would be expected leading to formation of $C^{16}O^{18}O$ as the product, whereas reversible oxidation and reduction of Pd by $^{16}O_2$ should not necessarily lead to isotopic scrambling. Therefore, it is anticipated that the degree of isotopic scrambling may provide some information on the relative importance of both storage mechanisms. The experimental result is shown in Fig. 7b: The CO_2 yield per pulse for $C^{16}O^{18}O$ amounts to approximately 5% of the $C^{16}O^{16}O$ yield throughout the entire experiment. In order to estimate the total quantity of oxygen withdrawn from the support, repeated pulsed CO titration experiments have consecutively been performed. The overall $C^{16}O^{18}O$ to $C^{16}O^{16}O$ ratio of these experiments is depicted in Fig. 7c. For the first experiments a steady decrease in $C^{16}O^{18}O$ formation is found whereas after about 10 titration experiments hardly any $C^{16}O^{18}O$ formation is observed anymore. (Note that 0.21% is the natural abundance of ^{18}O.) The total quantity of oxygen exchanged with the $Fe_3{}^{18}O_4$ film, which can be estimated by integrating over all titration experiments, amounts to the order of 10^{14} atoms cm^{-2}.

From the above results we conclude that the oxygen exchange kinetics between chemisorbed oxygen and Pd oxide on the one side and lattice oxygen from the support is very slow under the conditions applied in this study. From the total amount of oxygen exchange with the support, which is less than a monolayer, we can exclude that oxygen migration into the oxide support represents a major contribution to the storage mechanism. This is in agreement with PES spectra of the Fe 2p region showing no significant changes upon oxidation at 500 K. Interestingly, a significant oxygen exchange is only observed for the very first titration experiments. Recently we have shown that the model catalyst undergoes major structural changes during the first oxidation and reduction cycles, including an oxygen induced ripening of the Pd particles [31]. The number of oxidation/reduction cycles required to obtain a stable model surface coincides with the number of experiments showing an enhanced oxygen exchange. Therefore, it might be anticipated that initial restructuring of the catalyst may be connected to a strong interaction with the topmost support layer, possibly involving reaction and exchange of surface oxygen ions. However, the most important point to note is that in the stabilized state oxygen storage and release is predominantly facilitated by the formation and decomposition of Pd oxides.

3.4. Temperature dependence of surface oxidation

In the previous two paragraphs we have shown that for oxidation temperatures beyond 500 K, large amounts of Pd oxide can be formed on supported Pd nanoparticles. This oxide is preferentially formed at the particle/support interface, but generation of surface oxides is also possible. At 500 K oxygen exposure results in the formation of partially oxidized Pd particles, which mainly expose a metallic surface but also a minor fraction of surface oxides.

In order to study the formation of Pd surface oxides, we have investigated CO/O co-adsorption on partially oxidized Pd particles by IRAS over a broad temperature range. The pulse and temperature sequence of the corresponding experiments is illustrated in Fig. 8a: First, the reduced model surface is exposed to oxygen at different temperatures (8×10^{-7} mbar, 600 L, 1000 s), leading to partial oxidation. Subsequently, the sample is cooled in oxygen to 250 K to establish a saturated overlayer of chemisorbed oxygen on the remaining metallic Pd surface. After further cooling to 125 K in UHV, the sample is exposed to CO, leading to formation of a saturated CO/O co-adsorption layer. Finally, IRAS spectra of the co-adsorption layer are taken.

The corresponding IRAS spectra are shown in Fig. 8b as a function of oxidation temperature. As discussed in the previous paragraph, the spectra in the CO stretching frequency range show of a sharp peak at 2133 cm^{-1} and a broad feature at about 1960 cm^{-1}. In Fig. 8c the relative integral intensity in the CO stretching frequency region is shown normalized to a spectrum taken after oxygen exposure at 300 K (i.e. oxygen chemisorption only without formation of surface oxides). While no major differences in the spectra can be observed for oxidation temperatures up to approximately 475 K, the IR intensity of adsorbed CO decreases rapidly at higher oxidation temperatures. Oxidation at 600 K finally results in an almost complete quenching of the IR intensity for both CO-derived features. It is noteworthy that the shifts in the stretching frequencies for CO on the metallic Pd as a function of oxidation temperature are very small. Moreover, no additional peaks can be observed in the spectra which may be assigned to CO adsorption on the oxidized Pd.

As already addressed in the previous paragraph, the decreasing IR intensity for higher oxidation temperatures can be explained by the formation of Pd surface oxides. As a result the metallic Pd surface area shrinks which is available for CO adsorption. After oxidation at 600 K the CO signal from the metallic Pd surface is very small, indicating a nearly complete oxidation of the Pd surface. Nevertheless, no additional oxide-derived peaks appear in the IR spectra. Therefore, we conclude that CO does not adsorb on Pd surface oxides under the conditions applied in this study (125 K, $\sim 10^{-6}$ mbar). For oxidation temperatures below 475 K no major changes of the IR spectra are found while for higher temperatures the CO signal decreases due to the formation of surface oxides. Hence, the

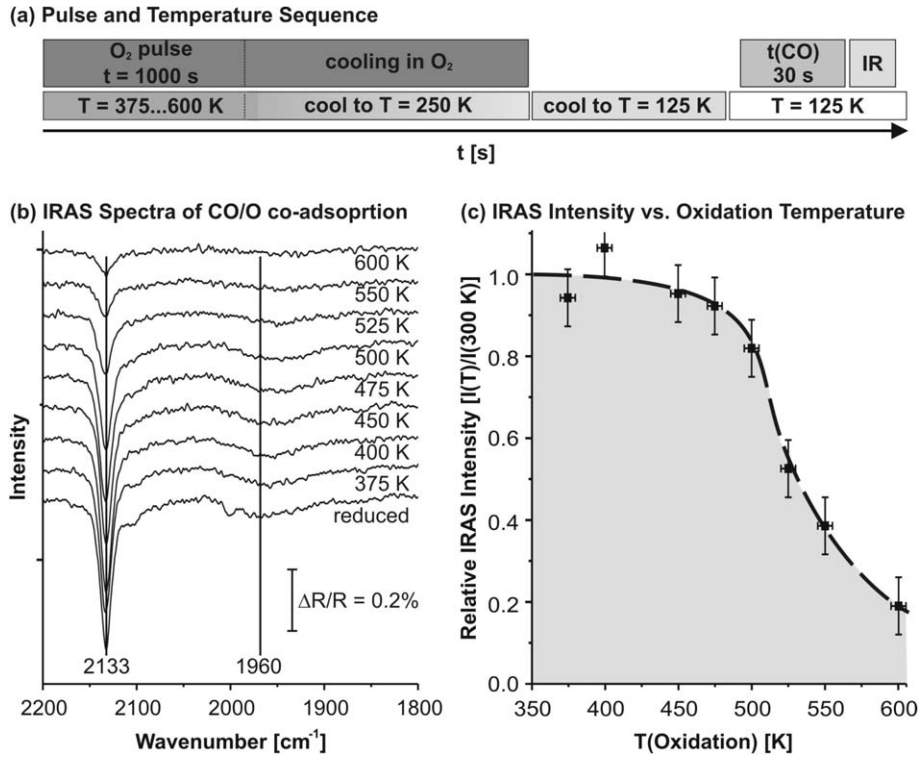

Fig. 8. (a) Pulse and temperature sequence of the IRAS experiments: First the sample is exposed to an O_2 pulse (8×10^{-7} mbar, 1000 s, 600 L) at different temperatures and subsequently cooled in O_2 to 250 K. After further cooling in UHV to 125 K, the sample is exposed to CO (8×10^{-7} mbar, 30 s, 18 L) and IR spectra are taken; (b) IRAS spectra of the CO stretching frequency region for CO/O co-adsorption on Pd/Fe_3O_4 at 125 K for different oxidation temperatures and (c) integral IRAS intensity normalized on the reduced surface as a function of oxidation temperature.

onset temperature of surface oxidation is found to be approximately 500 K. This result is in agreement with the CO titration experiments discussed above. As the IR intensity decreases steadily between 500 and 600 K, we suggest that in this temperature range metallic and oxidized surface areas co-exist on the Pd particles. Interestingly, oxidation at 525 K for 1000 s results in a much higher surface oxide coverage than even extended oxidation at 500 K. This effect may be addressed to different onset temperatures for oxidation of the various nonequivalent Pd surface sites. Briefly, the most import points to note are the increasing surface oxide formation for higher oxidation temperature and the fact that CO interaction with the surface oxide is very weak.

In addition to the formation of Pd surface oxides, we have also studied their reduction with CO. For this purpose, we have taken TR-IRAS spectra during reaction with CO exposure on a pre-oxidized sample. In Fig. 9a theses experiments are briefly summarized: Similar to all previous experiments, the sample is first oxidized by an O_2 pulse (1.7×10^{-6} mbar, 1300 L, 1000 s) at different sample temperatures. Next, that sample is cooled to 500 K in O_2. Afterwards, the sample is exposed to a continuous molecular beam of CO for 5400 s (4×10^{-6} mbar, 3 L/s) while TR-IRAS spectra of the CO stretching frequency region are recorded. The TR-IRAS spectra have been acquired by a remote-controlled routine with a time resolution of 20 s (128 scans per spectrum, 0.156 s per scan) for the first 10 spectra and 72 s (462 scans per spectrum, 0.156 s per scan) for the following 72 spectra. The result is displayed in Fig. 9b. Two bands are observed in the CO stretching frequency region at 1913 cm^{-1} and 1840 cm^{-1}. In Fig. 9b the temporal development of the CO signal during the reduction is depicted for a sample, which has been pre-oxidized at 600 K. A monotonously increasing intensity of both features with CO dosing time is found in the beginning which finally saturates after ~3000 s of CO exposure. The integral IR intensity of both CO features normalized with respect to CO adsorption on a reduced sample is shown in Fig. 9c as a function of CO exposure at different pre-oxidation temperatures. The initial IR intensity is found to be lower for higher oxidation temperatures. However, after different CO exposure times the IR intensity recovers to the level corresponding to the reduced surface. Surprisingly, the kinetics of the recovery of IR intensity is noticeably slower for higher oxidation temperatures as it can be derived from the steeper initial slope for lower oxidation temperatures in Fig. 9c.

As discussed in the previous paragraphs, no CO adsorption on Pd surface oxides was observed in this study even at low sample temperatures. Also, the CO spectra are very similar to the ones observed in previous in situ TR-IRAS studies on Pd model catalysts (for a detailed discussion and assignment see e.g. [22,35,44]). Consequently, we assign the signals in the CO stretching frequency region to the pseudo-steady-state coverage of CO adsorbed on metallic Pd under reaction conditions. The decrease in IR intensity after partial oxidation is due to a decreasing

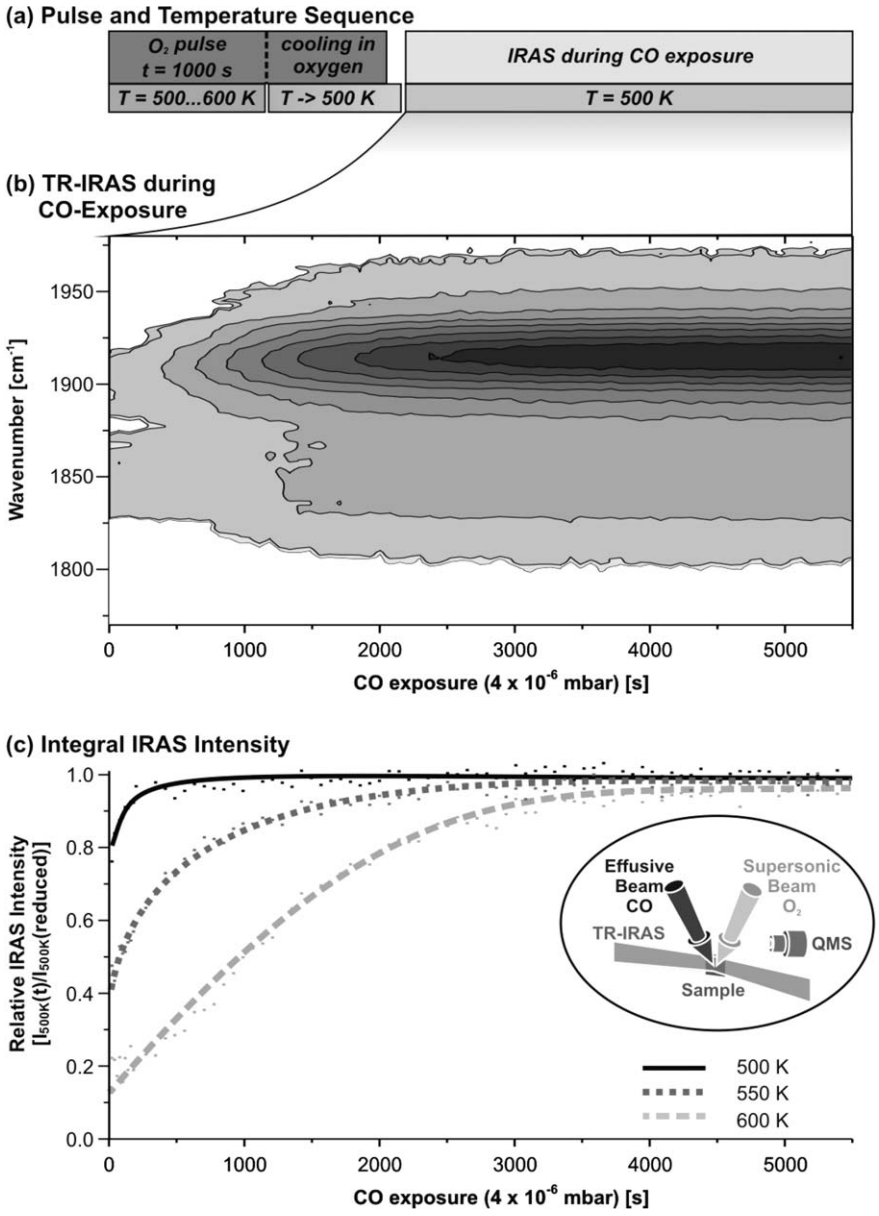

Fig. 9. (a) Pulse and temperature sequence of the in situ IRAS experiments: First the sample is exposed to an O_2 pulse (1.7×10^{-6} mbar, 1000 s, 1300 L) at different temperatures and cooled in O_2 to 500 K. Subsequently the sample is exposed to CO (4×10^{-6} mbar, 5400 s, ~15 000 L) and IR spectra are continuously acquired; (b) time resolved IRAS spectra showing the temporal development of the CO stretching frequency region during CO exposure after oxidation at 600 K and (c) time resolved integral IRAS intensity normalized on the reduced surface for different pre-oxidation temperatures.

amount of metallic Pd surface as a result of the formation of Pd surface oxides. Although IR intensity and CO adsorption are not directly proportional due to dipole coupling effects (see e.g. [45]), surface oxidation and reduction can be monitored at least qualitatively via TR-IRAS under reaction conditions. The decreasing CO signal with increasing oxidation temperature indicates an increasing coverage by surface oxides, in agreement with the CO/O co-adsorption experiments discussed above. The recovery of the initial CO signal after extended CO exposure indicates a reduction of the surface oxides. Two additional points are noteworthy here: First, for oxidation temperatures up to 600 K a complete reduction of Pd surface oxides can be obtained by extended CO exposure, indicated by the complete recovery of the CO signal to the level of the reduced surface. Hence, the formation of these surface oxides is a fully reversible process. Secondly, the reduction kinetics of such surface oxides is significantly slower for higher surface oxide coverages. This result is in agreement with pulsed CO titration experiments and transient molecular beam experiments, which show slower reaction kinetics for higher surface oxide coverages. This finding corroborates the above mentioned hypothesis that the reaction probability on the surface oxide is low and the reduction mainly occurs on the metallic part of the surface via decomposition of the oxide and reverse-spillover of oxygen from the oxide phase to the metallic Pd, followed by a Langmuir–Hinshelwood reaction on the metallic Pd.

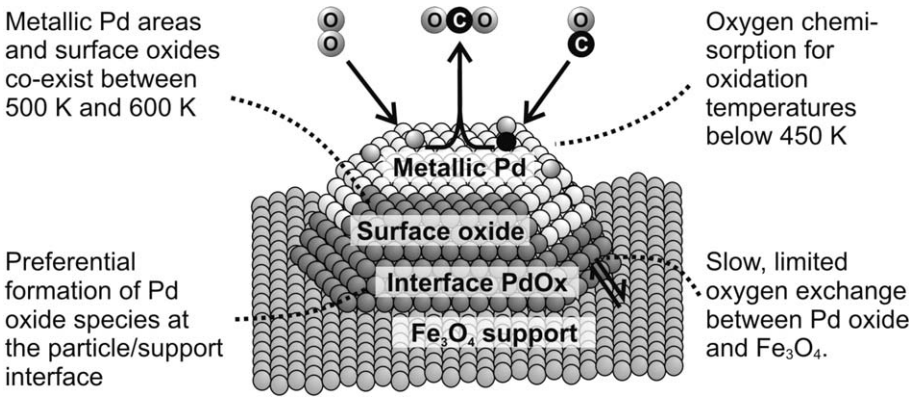

Fig. 10. Illustration of the oxygen storage and CO oxidation mechanism on the Pd/Fe_3O_4 supported model catalyst.

Detailed transient and pulsed MB experiments on the mechanism and the elementary kinetics will be presented in a forthcoming publication [36].

4. Conclusions

In this contribution we have studied in detail the interaction between oxygen and Pd nanoparticles (particle size 7 nm) supported on Fe_3O_4 over a broad temperature range. Combining fully automated multi-molecular beam experiments, TR-IRAS and PES, the formation of various oxygen species, surface and interface oxides was observed depending on the oxidation temperature:

1. *Chemisorbed oxygen ($T < 450$ K)*: Oxygen exposure at $\sim 10^{-6}$ mbar up to 450 K results in the formation of a dense chemisorbed oxygen layer on the metallic Pd surface, which is highly reactive towards CO oxidation. The density of adsorbed oxygen is limited and corresponds to the value expected for surface chemisorption on the basis of single crystal data.
2. *Pd interface oxide ($T > 500$ K)*: For oxidation temperatures of 500 K and above, initial oxidation of the Pd particles occurs in form of a thin Pd oxide layer at the particle/support interface. This oxide layer, which can be reversibly accumulated and depleted, acts as an oxygen reservoir providing oxygen for surface reactions. Large amounts of oxygen can be accumulated in the Pd particles without significant modifications of the metallic Pd surface. At 500 K, the maximum oxygen uptake corresponds to a formal stoichiometry of the particles of about $O/Pd = 0.55$. Limitations of oxygen formation can be addressed to strong kinetic hindrances inhibiting the oxidation process.
3. *Pd surface oxide ($T > 500$ K)*: In addition to the Pd interface oxide, the formation of surface oxides was also observed for temperatures above 500 K. With increasing oxidation temperatures an increasing fraction of the Pd surface becomes oxidized. While metallic Pd surface areas and surface oxides co-exist in the temperature range between 500 and 550 K, oxidation at 600 K results in a nearly complete surface oxidation. Formation of Pd surface oxides sensitively alters the adsorption properties of the catalyst, i.e. mainly due to very weak CO adsorption on the oxide phase. The reaction probability for CO oxidation on the Pd surface oxide is much lower than for the metallic surface covered by chemisorbed oxygen. A complete reduction of surface and interface oxides can be obtained by extended CO exposure.
4. *Oxygen storage in support lattice*: A slow and limited oxygen exchange between Pd oxide species and the Fe_3O_4 support has been observed. However, the total amount of oxygen that can be exchanged with the Fe_3O_4 lattice is small compared to the amount of Pd oxide species formed. It is most likely that the oxygen exchange is connected to a strong interaction with the topmost support layer connected to morphological changes of the catalyst surface.

In Fig. 10 a schematic model is depicted illustrating the different oxygen species observed in this study: For oxidation temperatures up to 450 K, oxygen mainly chemisorbs dissociatively on Pd particles. At oxidation temperatures of 500 K and above, initial oxidation of the Pd particles occurs by formation of a thin Pd oxide layer at the particle/support interface whereas with increasing oxidation temperatures the formation of Pd surface oxides has also been observed.

Acknowledgements

This work has been funded by the Deutsche Forschungsgemeinschaft (SPP 1091) and the Fonds der Chemischen Industrie. The authors are particularly grateful to the BESSY staff for technical support and to D.E. Starr and Sh.K. Shaikhutdinov for STM support.

References

[1] G. Ertl, H. Knoezinger, J. Weitkamp, in: G. Ertl, H. Knoezinger, J. Weitkamp (Eds.), Handbook of Heterogeneous Catalysis, VCH, Weinheim, 1997.

[2] J.M. Thomas, W.J. Thomas, Principle and Practice of Heterogeneous Catalysis, VCH, Weinheim, 1997.
[3] H. Conrad, G. Ertl, J. Küppers, E.E. Latta, Surf. Sci. 65 (1977) 245.
[4] R. Imbihl, J.E. Demuth, Surf. Sci. 173 (1986) 395.
[5] S.-L. Chang, P.A. Thiel, J. Chem. Phys. 88 (1988) 2071.
[6] X. Guo, A. Hoffman, J.T. Yates Jr., J. Chem. Phys. 90 (1989) 5787.
[7] V.A. Bondzie, P. Kleban, D.J. Dwyer, Surf. Sci. 347 (1996) 319.
[8] E.H. Voogt, A.J.M. Mens, J.W.G.O.L.J. Gijzeman, Surf. Sci. 373 (1997) 210.
[9] F.P. Leisenberger, G. Koller, M. Sock, S. Surnev, M.G. Ramsey, F.P. Netzer, B. Klötzer, K. Hayek, Surf. Sci. 445 (2000) 380.
[10] V.A. Bondzie, P.H. Kleban, D.J. Dwyer, Surf. Sci. 465 (2000) 266.
[11] G. Zheng, E.I. Altman, Surf. Sci. 462 (2000) 151.
[12] G. Zheng, E.I. Altman, Surf. Sci. 504 (2002) 253.
[13] E. Lundgren, G. Kresse, C. Klein, M. Borg, J.N. Andersen, M. De Santis, Y. Gauthier, C. Konvicka, M. Schmid, P. Varga, Phys. Rev. Lett. 88 (2002) 246103.
[14] M. Todorova, E. Lundgren, V. Blum, A. Mikkelsen, S. Gray, J. Gustafson, M. Borg, J. Rogal, K. Reuter, J.N. Andersen, M. Scheffler, Surf. Sci. 541 (2003) 101.
[15] E. Lundgren, J. Gustafson, A. Mikkelsen, J.N. Andersen, A. Stierle, H. Dosch, M. Todorova, J. Rogal, K. Reuter, M. Scheffler, Phys. Rev. Lett. 92 (2004) 046101.
[16] M. Todorova, K. Reuter, M. Scheffler, Phys. Rev. B 71 (2005) 195403.
[17] A. Stierle, N. Kasper, H. Dosch, E. Lundgren, J. Gustafson, A. Mikkelsen, J.N. Andersen, J. Chem. Phys. 122 (2005) 44706.
[18] H. Over, M. Muhler, Prog. Surf. Sci. 72 (2003) 3.
[19] G. Zheng, E.I. Altmann, J. Phys. Chem. B 2002 (2002) 1048.
[20] B.L.M. Hendriksen, S.C. Bobaru, J.W.M. Frenken, Surf. Sci. 552 (2004) 229.
[21] H.-J. Freund, Catal. Today 100 (2005) 3.
[22] J. Libuda, H.-J. Freund, Surf. Sci. Rep. 57 (2005) 157.
[23] C.R. Henry, Surf. Sci. Rep. 31 (1998) 231.
[24] V.P. Zhdanov, B. Kasemo, Surf. Sci. Rep. 39 (2000) 25.
[25] T.P. St. Clair, D.W. Goodman, Top. Catal. 13 (2000) 5.
[26] H.-J. Freund, M. Bäumer, J. Libuda, T. Risse, G. Rupprechter, S. Shaikhutdinov, J. Catal. 216 (2003) 223.
[27] T. Schalow, M. Laurin, B. Brandt, S. Schauermann, S. Guimond, H. Kuhlenbeck, D.E. Starr, S.k. Shaikhutdinov, J. Libuda, H.-J. Freund, Angew. Chem. Int. Ed. 44 (2005) 7601.
[28] J. Libuda, I. Meusel, J. Hartmann, H.-J. Freund, Rev. Sci. Instrum. 71 (2000) 4395.
[29] W. Weiss, W. Ranke, Prog. Surf. Sci. 70 (2002) 1.
[30] C. Lemire, R. Meyer, V. Henrich, S.K. Shaikhutdinov, H.-J. Freund, Surf. Sci. 572 (2004) 103.
[31] T. Schalow, B. Brandt, D.E. Starr, M. Laurin, S. Schauermann, S.K. Shaikhutdinov, J. Libuda, H.-J. Freund, Catal. Lett. 107 (2006) 189.
[32] T.W. Orent, S.D. Bader, Surf. Sci. 115 (1982) 323.
[33] A.M. Bradshaw, F.M. Hoffman, Surf. Sci. 72 (1978) 513.
[34] L. Piccolo, C. Becker, C.R. Henry, Appl. Surf. Sci. 164 (2000) 156.
[35] J. Libuda, I. Meusel, J. Hoffmann, J. Hartmann, L. Piccolo, C.R. Henry, H.-J. Freund, J. Chem. Phys. 114 (2001) 4669.
[36] T. Schalow, B. Brandt, S. Schauermann, J. Libuda, H.-J. Freund, in preparation.
[37] D.A. King, M.G. Wells, Proc. Roy. Soc. Lond., Ser. A 339 (1974) 245.
[38] D.A. King, M.G. Wells, Surf. Sci. 29 (1972) 454.
[39] J. Mendez, S.H. Kim, J. Cerda, J. Wintterlin, G. Ertl, Phys. Rev. B 71 (2005) 085409.
[40] X. Xu, D.W. Goodman, J. Phys. Chem. 97 (1993) 7711.
[41] S. Tanuma, C.J. Powell, D.R. Penn, Surf. Interf. Anal. 17 (1991) 927.
[42] J.N. Andersen, D. Hennig, E. Lundgren, M. Methfessel, R. Nyholm, M. Scheffler, Phys. Rev. B 50 (1994) 17525.
[43] H. Gürer, K. Klier, G.W. Simmons, Phys. Rev. B 49 (1994) 14657.
[44] I. Meusel, J. Hoffmann, J. Hartmann, J. Libuda, H.-J. Freund, J. Phys. Chem. B 105 (2001) 3567.
[45] F.M. Hoffmann, Surf. Sci. Rep. 3 (1983) 107.